

Visual-Friendly Concept Protection via Selective Adversarial Perturbations

Xiaoyue Mi, Fan Tang, Juan Cao, Peng Li, Yang Liu

Abstract—Personalized concept generation by tuning diffusion models with a few images raises potential legal and ethical concerns regarding privacy and intellectual property rights. Researchers attempt to prevent malicious personalization using adversarial perturbations. However, previous efforts have mainly focused on the effectiveness of protection while neglecting the visibility of perturbations. They utilize global adversarial perturbations, which introduce noticeable alterations to original images and significantly degrade visual quality. In this work, we propose the Visual-Friendly Concept Protection (VCPro) framework, which prioritizes the protection of key concepts chosen by the image owner through adversarial perturbations with lower perceptibility. To ensure these perturbations are as inconspicuous as possible, we introduce a relaxed optimization objective to identify the least perceptible yet effective adversarial perturbations, solved using the Lagrangian multiplier method. Qualitative and quantitative experiments validate that VCPro achieves a better trade-off between the visibility of perturbations and protection effectiveness, effectively prioritizing the protection of target concepts in images with less perceptible perturbations. Our code is available at <https://github.com/KululuMi/VCPro>.

Index Terms—Unauthorized personalizations, Adversarial Attacks, Diffusions, Privacy protections, Copyright protections.

I. INTRODUCTION

With the advent of popular image generative models [1]–[3] such as Stable Diffusion [2] and GPT-4o [4], people lacking expertise in drawing or photography can effortlessly create realistic or artistic works using simple textual descriptions. However, the success of these models has raised significant concerns about privacy, intellectual property rights, and various legal and ethical issues [5]. For example, an adversary could easily generate sensitive specific concepts, such as personal fake images, or imitate renowned artworks for commercial purposes, using only a few reference images and concept personalization techniques such as Textual Inversion [6] or DreamBooth [7].

One prevailing direction to mitigate these potential risks is to leverage adversarial attack techniques, transforming original images into adversarial examples, termed “protected images”. These protected images can misguide the personalized diffusion model and deceive its generation process, which resists malicious editing or personalization [8], [10], [12]–[15]. For instance, AdvDM [13] employs adversarial attacks in the inversion stage of Stable Diffusion to safeguard against malicious imitation of the style of a specific artist. Later, its

Xiaoyue Mi, Fan Tang, and Juan Cao are with the Institute of Computing Technology, Chinese Academy of Sciences, China, and also with the University of Chinese Academy of Sciences, China (e-mail: mixiaoyue19s@ict.ac.cn; tfan.108@gmail.com; caojuan@ict.ac.cn)

Peng Li and Yang Liu are with Tsinghua University, China (e-mail: pengli09@gmail.com; liuyang2011@tsinghua.edu.cn)

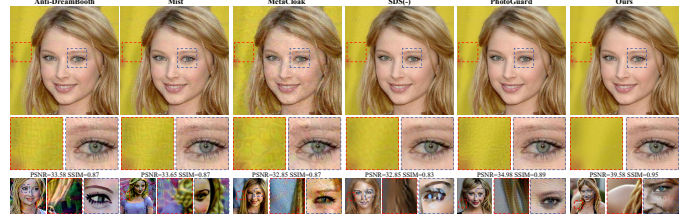


Fig. 1. The first row shows protected images from Anti-DreamBooth [8], Mist [9], MetaCloak [10], SDS(-) [11], PhotoGuard [12], and our VCPro. The second row highlights magnified background and face regions, while the third row presents Textual Inversion results. With 8/255 perturbation size, our method achieves a better balance between protection effectiveness and visual quality for user-important concepts, as shown by higher PSNR/SSIM values.

updated version, Mist [14], enhances the protection efficacy of protected images by adding a textual loss, extending its application from Textual Inversion to DreamBooth. Unlike AdvDM and Mist, which focus on art style protection, Anti-DreamBooth [8] undermines DreamBooth model generation quality to enhance privacy by adding adversarial perturbations to human face images before posting online. Furthermore, MetaCloak [10] leverages a meta-learning strategy and data transformations to generate more effective and robust protected images against DreamBooth.

However, these methods primarily focus on preventing the personalization methods from generating high-quality corresponding images, often resulting in noticeable and unacceptable perturbations. They usually use 11/255 [8], [10], [15] or 17/255 [14] as perturbation size in their paper, which is generally unacceptable for owners of face photos, significantly limiting the usability of these methods in real-world applications. Therefore, we pose the following question in this work: *How can we find a better trade-off between visibility of perturbations and protection effectiveness?*

To answer this question, we highlight the sparsity of images under concept protection tasks: The critical information that deserves protection constitutes only a part of the image. Previous approaches aim to protect the entire image, including background regions and other non-essential information, enhancing the visibility of perturbations. As shown in Fig. 1, the protected images generated by Mist, Anti-DreamBooth, MetaCloak, SDS(-), and PhotoGuard, exhibit noticeable odd textures on the entire image: face, neck, and background, and their final protective effects akin to a special style picture of the target person. In contrast, we prioritize protecting essential information within an image, utilizing a more stealthy adversarial perturbation.

To this end, we introduce a Visual-Friendly Concept Protection (VCPro) framework to counteract unauthorized concept-driven text-to-image synthesis. This framework learns

selective adversarial perturbations targeting important regions. Unlike discriminative tasks where important information is class-related and provided by target model gradients, identifying crucial information in generative tasks is challenging. VCPro utilizes user-provided masks for target concept protection, which can be supplemented by other privacy detection tools for online platforms. In that way, we propose a regional adversarial loss using spatial information to focus on selected areas. To further enhance visual quality, we apply a Lagrangian multiplier-based solution, shifting from maximizing protection effectiveness to minimizing perceptibility while ensuring effective protection. Considering human sensitivity to low-frequency changes, we measure perturbation perceptibility in the frequency domain. Experiments on models like Textual Inversion and DreamBooth validate VCPro’s effectiveness. Our approach yields subtler adversarial perturbations compared to baselines like Mist and Anti-DreamBooth, especially FID, which is reduced from 96.24 to 27.04.

Our contributions are summarized as follows:

- We point out that the existing image protection methods over-emphasize the final protection effectiveness while neglecting the visual appearance of the protected images.
- We propose a visual-friendly concept protection framework to prioritize protecting essential information within images by a regional adversarial loss and loosen the optimization objective from finding the strongest perturbations within the perturbation size to the smallest feasible perturbations.
- Experiments demonstrate that our approach can focus on crucial concepts specified by users with lower perceptibility than baselines, achieving a better trade-off between protection effectiveness and perturbation visibility.

II. RELATED WORK

Personalization of Diffusions Models. Personalization for specific concepts (attributions, styles, or objects) has been a long-standing goal in the image generation field. In text-to-image diffusion models, previous researchers have primarily concentrated on prompt learning and test-time tuning of pre-trained models to generate images based on specific target concepts using special language tokens. Textual Inversion adjusts text embeddings of a new pseudoword to describe the concept [6]. DreamBooth fine-tunes denoising networks to connect the novel concept and a less commonly used word token [7]. Based on that, more works [16]–[18] are proposed to improve controllability and flexibility in processing image visual concepts. In this paper, we have selected Textual Inversion and DreamBooth as the techniques used by the adversary due to their popularity and representativeness.

Imperceptibility Adversarial Attack. Adversarial examples [9], [19]–[22] are initially introduced by adding imperceptible noise to original data, fooling classifiers into misclassifying with high confidence. Recently, more and more researchers aim to improve the imperceptibility of adversarial examples, and they make use of a variety of tools such as perceptual color distance [23], low-frequency spatial constraints [24], hybrid attacks in frequency and spatial domain [25], and

invertible neural networks [26], etc. But they are mainly aimed at discriminative tasks such as image classification, where important information in the image can be fed back relatively accurately by the gradient of the target model, whereas we target a diffusion-based generative model whose gradient is also for the whole image.

Adversarial Examples Against Unauthorized AI Generation. Unauthorized AI Generation seriously harms the safety of society, prompting researchers to explore multiple approaches for mitigating these risks. While passive defense methods focus on distinguishing between authentic and synthetic images [27], [28], adversarial attacks are a promising way against unauthorized AI generation [29]–[32]. Ruiz *et al.* [29] are the first to adapt adversarial attack methods to undermine the generation of realistic deepfake images, thereby enhancing privacy security. Anti-Forgery [30] computes adversarial noise in the Lab color space to enhance the imperceptibility and robustness of various image transformations. Unlike others, DeepFake Disrupter [31] generates adversarial noise using an autoencoder instead of gradients and spoofs deepfake generators while remaining undetected by deepfake detectors. Zhu *et al.* [32] utilize adversarial examples to protect images while simultaneously recovering original image information from tampered images. In contrast to discriminative tasks, adversarial examples play a positive role in the image generation field.

With the rising popularity of diffusion models, previous works are difficult to adapt due to the obvious differences between diffusion and GAN or other generation models. Therefore, there is a growing interest in using adversarial examples to protect images from being maliciously exploited by diffusion models [10], [12], [13]. Photoguard [12] attacks the VAE encoder or whole model to prevent images from being maliciously edited by diffusion models at the test time. At the same time, AdvDM [13] employs adversarial examples to protect artists from having their styles imitated by textual inversion by maximizing the denoising loss of a pre-trained diffusion model. As an upgraded version of AdvDM, Mist [14] adds a texture loss that measures the distance between the encoder representation of the original image and the perturbed image in the image encoder of latent diffusion. Similar to them, GLAZE [15] proposes to measure the art style similarity between the perturbed image and the target style using a pre-trained style-transfer model, and adversarial examples can protect the art style-related attributes in the original image directly. Different from them, Anti-DreamBooth [8] protects privacy information from being learned by DreamBooth. Based on that, MetaCloak [10] uses a meta-learning strategy and data transformations to generate better effective and robust adversarial examples. Meanwhile, Xue *et al.* [11] introduce Score Distillation Sampling (SDS) loss into the perturbation optimization process to reduce computation cost and find maximize or minimize SDS loss both achieve competitive protection effects.

However, except for GLAZE, existing work protects all information for the whole image, which often requires significant noise, significantly affects the user experience, and may overemphasize the background, omitting the information that

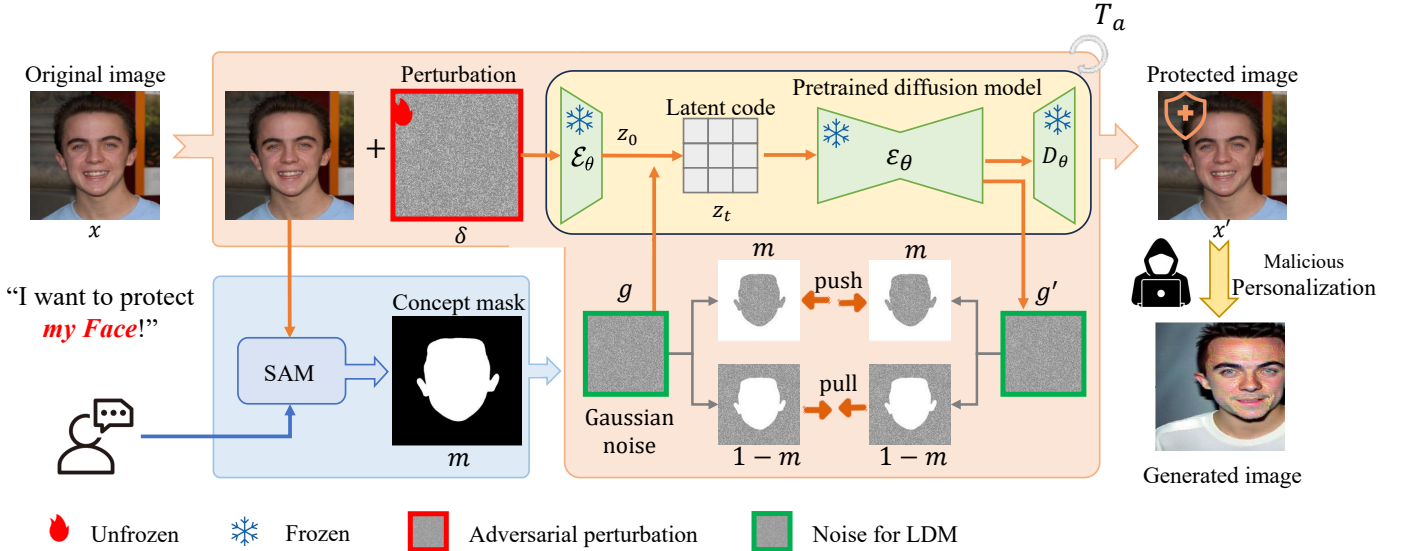


Fig. 2. The pipeline of VCPRO. Initially, users can utilize SAM or alternative segmentation tools to create user-protective masks within images. Following this, the masks and the original images are simultaneously input into the protected image generation module, as described by Eq. (8). Within this module, we introduce a regional adversarial learning loss aimed at diminishing the visibility of protected images by precise protection and transform objectives to minimize perturbations while maintaining effective protection.

needs to be protected. In our work, we propose to prioritize limited noise to protect important information in the image, such as faces, and specific IPs. Unlike GLAZE which targets art style, we target specific semantic regions.

III. PRELIMINARIES

Personalization based on Diffusion. Concept-driven personalization customizes the outputs of a generative model to align with a specific concept, such as attributes, style, objects, etc. Most personalization techniques are applied to the latent diffusion model (LDM, parameterized by θ). A typical LDM consists of an image encoder \mathcal{E}_θ , an image decoder \mathcal{D}_θ , a condition encoder τ_θ , and a conditional denoising UNet ε_θ . The training of LDMs contains diffusion and denoising processes, which both happen in the latent space. For an image x , $z_0 = \mathcal{E}_\theta(x)$ is the latent code of x . The diffusion process randomly samples time t and Gaussian noise g , and latent vector z_0 is added noise g to z_t . Then the denoising UNet ε_θ is assigned to remove the noise added to the latent code z_t conditioned by $\tau_\theta(y)$ in each timestep t , and we set the output of ε_θ as g' . The training objective of this LDM is:

$$\mathcal{L}_\theta := \mathbb{E}_{z \sim \mathcal{E}(x), y, g \sim \mathcal{N}(0,1), t} \left[\|g - \varepsilon_\theta(z_t, t, \tau_\theta(y))\|_2^2 \right], \quad (1)$$

where t is a timestep of the diffusion process, and y is the given condition for generation.

Based on LDM, Textual Inversion, and DreamBooth are two main techniques for personalization. Textual Inversion learns new special tokens containing specific concepts to store new knowledge from images. In Textual Inversion, y usually is a generic prompt, such as “a photo of sks [class noun]”, with sks is a pseudo token, and “[class noun]” is the object type. They optimize the embedding of sks directly by minimizing the objective specified in Eq. (1), which uses a small set of images representing the concept as training data.

$$\arg \min_v \mathbb{E}_{z, y, g, t} \left[\|g - \varepsilon_\theta(z_t, t, \tau_\theta(y))\|_2^2 \right]. \quad (2)$$

DreamBooth also binds new conceptual knowledge to specific words. Unlike Textual Inversion, it fine-tunes part of the parameters of LDMs on training images and class examples x^p , which is generated from original LDM with prior prompt y^p to mitigate catastrophic forgetting.

$$\theta := \arg \min_\theta \mathbb{E}_{z, y, g, t} \left[\|g - \varepsilon_\theta(z_t, t, \tau_\theta(y))\|_2^2 + \|g - \varepsilon_\theta(z_t^p, t^p, \tau_\theta(y^p))\|_2^2 \right]. \quad (3)$$

Protected Image for Diffusions. Protected images (adversarial examples) aim to add an imperceptible adversarial perturbation δ to the original image x to make the full process of condition generation ineffective. The protected image \mathcal{L}_θ can be formalized as:

$$\begin{aligned} x' &:= \arg \max_{x'} \mathcal{L}_\theta(x', y), \\ \text{s.t. } &\|x - x'\| \leq \epsilon, \end{aligned} \quad (4)$$

where ϵ is the perturbation size, also known as the perturbation budget, and limits the maximum range of adversarial perturbation. Adversarial attack transforms original images into special samples that are difficult to denoise. They enhance the optimization challenge of LDMs, thereby achieving image protection.

IV. VISUAL-FRIENDLY CONCEPT PROTECTION

A. Overview

Fig. 2 shows the pipeline of the proposed framework for visual-friendly concept protection. Accurately describing spatial positions through language can be challenging for users, but it can be precisely achieved using masks. By leveraging SAM [33] or other segmentation tools, users can generate a mask m for important concepts within a given image x . The user-provided masks and original images are then collectively fed into the protected image generation module

as described in Eq. (8). In this module, we propose a regional adversarial learning loss to reduce the visibility of protected images through precise protection and a Lagrangian multiplier-based solution to minimize perturbations while maintaining successful protection.

In this section, we start by formulating the regional adversarial learning framework for diffusion models in Sec. IV-B and then move on to the solution of the proposed optimization objectives in Sec. IV-C. The total learning process is shown in Alg. 1.

B. Formulation

Regional Adversarial Loss. Unlike previous studies, we aim to achieve precise concept protection to reduce the perceptibility of protected images. We use mask m to indicate the spatial positions of important information in the feature map enabling precise concept protection. This precise optimization allows prioritized protection of the most critical information in the image with a smaller adversarial perturbation. The optimization objective of protected images in our method can be defined as:

$$\begin{aligned} x' &:= \arg \max_{x'} \mathcal{L}'_{\theta}(x', y, m), \\ \text{s.t.} \quad & \|x - x'\| \leq \epsilon, \end{aligned} \quad (5)$$

and the regional adversarial loss \mathcal{L}'_{θ} combines a “push” term for protected regions and a “pull” term for non-protected regions.

$$\mathcal{L}'_{\theta} := \mathbb{E}_{z \sim \mathcal{E}(x), y, g \sim \mathcal{N}(0,1), t} [l_{mask}(z_t, y, g, t, m)], \quad (6)$$

$$\begin{aligned} l_{mask}(z_t, y, g, t, m) &:= \underbrace{\|(g - \varepsilon_{\theta}(z_t, t, \tau_{\theta}(y))) \odot m\|_2^2}_{\text{push term for protected regions}} \\ &\quad - \underbrace{\|(g - \varepsilon_{\theta}(z_t, t, \tau_{\theta}(y))) \odot (1 - m)\|_2^2}_{\text{pull term for non-protected regions}}. \end{aligned}$$

This loss operates through a balanced mechanism of opposing forces. The push term maximizes the distance between the predicted noise ε_{θ} and ground truth noise g in masked regions ($m = 1$), effectively disrupting the denoising process for protected concepts. Simultaneously, the pull term minimizes this distance in unmasked regions ($m = 0$), preserving visual quality in non-protected areas.

During optimization, these components generate distinct gradient signals: push gradients divert predictions away from ground truth in protected regions, while pull gradients maintain accuracy elsewhere. This dual approach is crucial for effective protection—without the pull component, regions outside the mask cannot provide sufficient gradient feedback, significantly impairing the optimization process. Our ablation studies in Fig. 4 and Table II demonstrate that removing the pull component substantially degrades protection effectiveness.

C. Lagrangian Multiplier-based Loose Solution

Based on Eq. (6), protected images will destroy the target area as much as possible. However, for the generation task, the output can still be recognized as synthetic as long as there are some clear signs of protection. Typical image classification

Algorithm 1 Visual-Friendly concept protection (VCPro) framework

Require: Image x , diffusion model with parameter θ , number of time steps T , text condition y , attack steps T_a , step size α , and adversarial perturbation size ϵ

- 1: Initialize $x' = x$, $i = 0$
 - 2: Get mask m by SAM or user-provide
 - 3: **while** $i < T_a$ **do**
 - 4: Sample $t \sim [0, T]^n$
 - 5: $\delta = \text{Uniform}(-\epsilon, \epsilon)$
 - 6: Calculate $\mathcal{L}_{final}(x', y, m)$ by Eq. (8)
 - 7: $\delta = \delta - \alpha \cdot \text{sign}(\nabla_{\delta} \mathcal{L}_{final}(x', y, m))$
 - 8: $\delta = \max(\min(\delta, \epsilon), -\epsilon)$
 - 9: $x' = x' + \delta$
 - 10: $x' = \max(\min(x', 255), 0)$
 - 11: $i = i + 1$
 - 12: **end while**
 - 13: **return** Protected image x'
-

attacking methods [20], [24], [26] also present similar viewpoints that minimize the impact on normal visual perception while maintaining the effectiveness of the attack. Hence, we propose a loosed optimization objective by attempting to find the minimal adversarial perturbation δ that can attack diffusion models successfully. For convenience, we set a heuristic method: if $\mathcal{L}'_{\theta} > \alpha$, the attack is successful. The problem can be translated as:

$$\begin{aligned} &\text{minimize} && D(x, x + \delta), \\ &\text{such that} && -\mathcal{L}'_{\theta} + \alpha \leq 0, \\ & && \delta \in [-\epsilon, \epsilon]^n, \\ & && x + \delta \in [0, 255]^n, \end{aligned} \quad (7)$$

where $D(\cdot)$ is a distance metric.

For ease of solution, we use Lagrangian multiplier method and get the alternative formulation:

$$\begin{aligned} &\text{minimize} && \mathcal{L}_{final} = c \cdot D(x, x + \delta) - \mathcal{L}'_{\theta} + \alpha, \\ &\text{such that} && \delta \in [-\epsilon, \epsilon]^n, \\ & && x + \delta \in [0, 255]^n, \end{aligned} \quad (8)$$

where a constant $c > 0$ is appropriately selected. The equivalence of Eq. (7) and Eq. (8) can be understood by the existence of a positive constant c ensuring the best solution for the second formulation aligns with that of the first.

Considering that the human visual system is more sensitive to low-frequency regions [24], we use $D(\cdot)$ to limit perturbations into the high-frequency regions. Specifically, we use discrete wavelet transform (DWT) to transform images from the spatial domain to the frequency domain. DWT will decompose the image x into one low-frequency and three high-frequency components, i.e., $x_{ll}, x_{lh}, x_{hl}, x_{hh}$, and inverse DWT (IDWT) uses all four components to reconstruct the image.

$$\begin{aligned} x_{ll} &= LxL^T, & x_{lh} &= HxL^T, \\ x_{hl} &= LxH^T, & x_{hh} &= HxH^T, \end{aligned}$$

where L and H are an orthogonal wavelet’s low-pass and high-pass filters, respectively. x_{ll} preserves the low-frequency information of the original image, whereas x_{lh} , x_{hl} and x_{hh} are associated with edges and drastic variations.

In this work, we drop the high-frequency components and reconstruct an image with only the low-frequency component as $\tilde{x} = \phi(x)$, where $\phi(x) = L^T x_{ll} L = L^T (LxL^T)L$, and $D(\cdot) = \|\tilde{x} - x'\|_2^2$.

V. EXPERIMENTS

This section introduces our experimental settings and qualitative and quantitative experiments to demonstrate our effectiveness in generating protected images with less visual perceptibility while safeguarding key concepts in user-provided images.

A. Experimental Settings

Datasets. We used the CelebA-HQ [34] and VGGFace2 [35] datasets, following Anti-DreamBooth [8] and MetaCloak [10], to validate the effectiveness of our method in privacy protection. CelebA-HQ is an enhanced version of the original CelebA dataset consisting of 30,000 celebrity face images. VGGFace2 is a large-scale dataset with over 3.3 million face images from 9,131 unique identities. We randomly selected 50 identities from each dataset, ensuring that each had at least 15 images with a resolution exceeding 500×500 pixels. We also provide other non-face cases (artwork and landscape) in the paper.

Training details. The availability of Stable Diffusion pre-trained weights on Hugging Face ¹ has significantly advanced research within the community. Here, our experiments primarily focus on the Stable Diffusion v1-4 version. For image pre-processing, we center crop and resize images to a resolution 512×512 . During protected image generation, we use 720 iterations, step size α is $1/255$, and adversarial perturbation size ϵ is $8/255$. We test the protection performance on two types of SOTA personalization methods, i.e., Textual Inversion (TI) [6], and DreamBooth (DB) [7]. During the training of the Textual Inversion, the constant learning rate is set to 5×10^{-4} with 3000 optimization steps and batch size 1. In DreamBooth, the constant learning rate is set to 5×10^{-7} with 1000 optimization steps and batch size is 2. We use a guidance scale of 7.5 and 50 denoising steps at the generation phase with a testing prompt. We set $c = 0.1$ and $\alpha = 0.5$ in practice. All experiments are complete on NVIDIA A100 GPU 40GB.

Baselines. We compare our method with five SOTA baselines, i.e., Mist [13], Anti-DreamBooth (referred to as Anti-DB) [8], PhotoGuard [12], SDS(-) [11] and MetaCloak [10]. In implementations, we set $\epsilon = 8/255$ as the ℓ_∞ perturbation size, $\alpha = 1/255$ as the step size for fair comparison.

- Mist aims to maximize the training loss of Latent Diffusion Models (LDMs) while minimizing a textual loss between the protected image and a dummy image in the image encoder layer during protected image generation.

In our implementation, following the original paper [14], we set the loss weight for the textual loss to 1×10^{-4} and run 720 iterations during protected image generation.

- Anti-DreamBooth focuses on maximizing the training loss of LDMs to generate protected images. We use the most visually imperceptible variant, FSMG, which employs a DreamBooth model trained on original images for protected data generation. The adversarial iterations were set to 720.
- PhotoGuard targets diffusion-based inpainting/editing methods and offers two variants: one that attacks the VAE-encoder of LDMs, and another that attacks the final image outputs. We select the VAE-encoder variant due to its superior visual quality and set the training iterations to 200, as recommended in the original paper [12].
- SDS(-) minimizes the SDS loss [36] to optimize adversarial data, achieving the best visual quality among all versions presented in its original paper [11]. We set the training iterations to 100, following [11].
- MetaCloak utilizes meta-learning to enhance the robustness of adversarial data against various transformations. We set the number of surrogate models to 5, the unrolling number to 1, the sample batch size to 1, and the training iterations to 4000, based on the recommendations in [10].

Metrics. To measure the visual perception of protected data, we calculate the FID [37], SSIM [38], and PSNR between protected and original images. The goal of the protection is to reduce the visual quality of generated images when adversaries use Textual Inversion and DreamBooth for personalization generation. So we use a full image quality evaluation metric LIQE [39] and propose a face regional quality evaluation metric CLIP-FACE [10] as automatic evaluation metrics to assess protection effectiveness. LIQE is an advanced blind image quality assessment tool that measures image quality on a five-point scale: $c \in C = \{1, 2, 3, 4, 5\} = \{\text{“bad”}, \text{“poor”}, \text{“fair”}, \text{“good”}, \text{“perfect”}\}$. CLIP-FACE is based on CLIP-IQA [40] for visual quality by considering additional class information. Specifically, we calculate the CLIP score difference between “good face” and “bad face”. Considering the large number of images generated by Textual Inversion or DreamBooth, fine-grained labeling of facial regions in every image and then evaluating them is expensive. CLIP-FACE uses the multimodal understanding capability of CLIP and can focus on the facial regions in a coarse-grained manner. To assess the efficacy of the protection mechanism, we generate 16 images for each trained Textual Inversion model and DreamBooth model with testing prompt “a photo of *sk*s person” or “a photo of *sk*s object”. As image quality assessment remains a challenging problem, particularly with the lack of precise concept-specific automated metrics, we also provide human evaluation to assess the visual perception of protected data and the efficacy of safeguarding the target concepts.

B. Main Results

Quantitative Results. Table I shows the automatic and human evaluation results for the visibility of protected images and the final protection effectiveness of different methods.

¹<https://huggingface.co/>

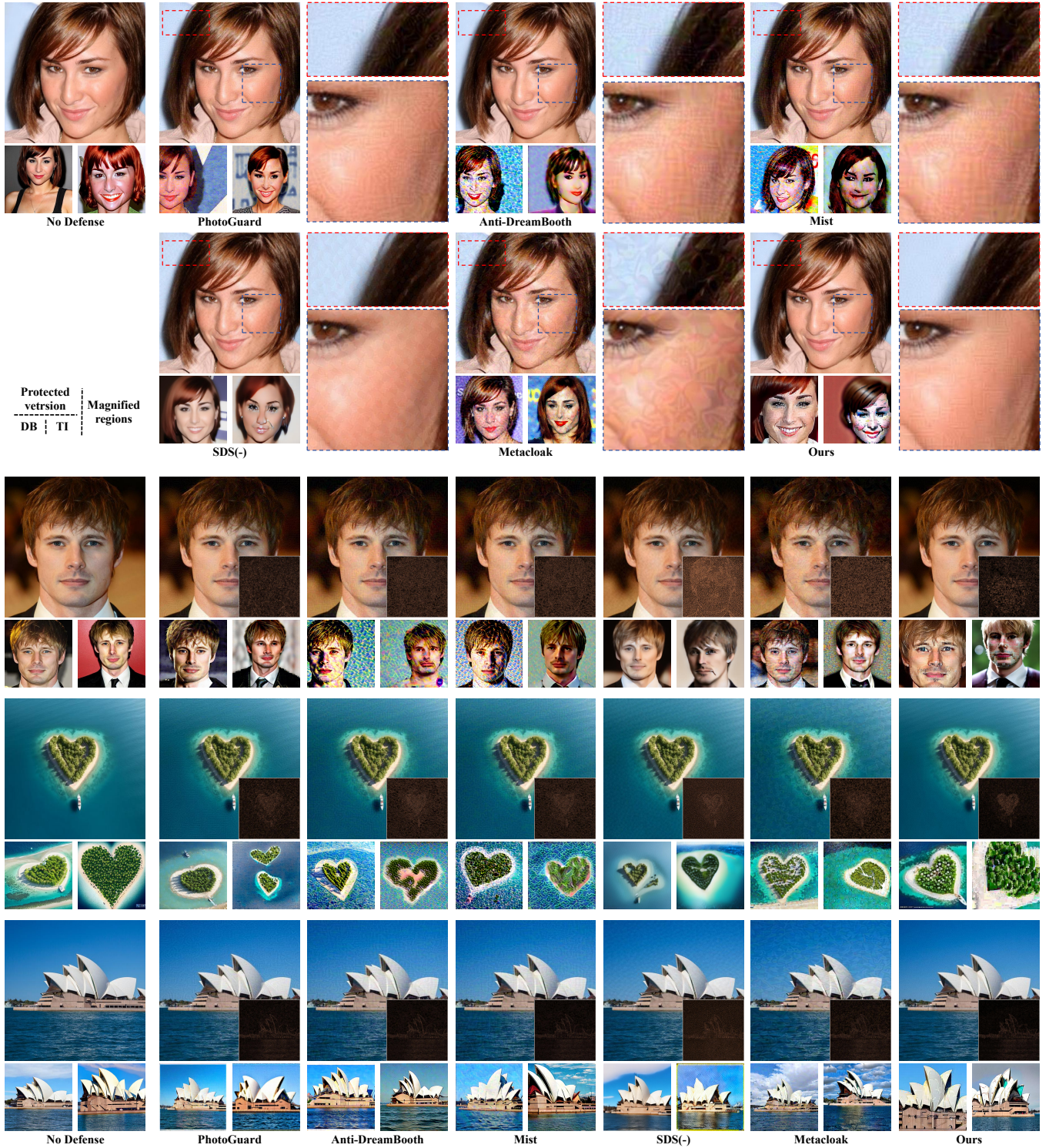


Fig. 3. Qualitative defense results for both the human face and non-face cases. For generating protected images, we use an ϵ value of $8/255$ with Stable Diffusion v1-4. Each row displays the original images (No Defense), the protected images generated by PhotoGuard, Anti-DreamBooth, Mist, SDS(-), MetaCloak, and our method, along with their respective outcomes in Textual Inversion (TI) and DreamBooth (DB). Additionally, we include visualizations of adversarial perturbations represented as black-yellow images. For better detail, please zoom in.

TABLE I

AUTOMATIC AND HUMAN EVALUATIONS ACROSS DIFFERENT METHODS, INCLUDING THEIR RESPECTIVE MEAN AND STANDARD DEVIATION (\pm) ON THE VGGFACE2 AND CELEBA-HQ DATASETS. ALL METHODS EMPLOYED A PERTURBATION SIZE OF $\epsilon = 8/255$. IN THE HUMAN EVAL RESULTS, "LOSS/TIE/WIN" IN "VISIBILITY" INDICATES THE VOTING RATES FOR VCPro LOSSES, TIES, AND WINS IN COMPARISON TO OTHER METHODS REGARDING THE STEALTHINESS OF THEIR ADVERSARIAL PERTURBATIONS. "TI/DB" REPRESENTS THE PERCENTAGE OF IMAGES GENERATED BY TEXTUAL INVERSION/DREAMBOOTH IDENTIFIED AS SYNTHETIC. \uparrow MEANS THE HIGHER THE BETTER, AND VICE VERSA. THE BEST RESULT IN EACH COLUMN IS IN BOLD.

Methods	Publication	Visibility of Perturbations			Textual Inversion		DreamBooth		HumanEval			
		FID \downarrow	SSIM \uparrow	PSNR \uparrow	LIQE \downarrow	CLIP-FACE \downarrow	LIQE \downarrow	CLIP-FACE \downarrow	Visibility (Loss/Tie/Win)	TI \uparrow	DB \uparrow	
VGGFace2	No Defense	-	-	-	3.61 \pm 0.98	0.24 \pm 0.34	3.95 \pm 1.11	0.38 \pm 0.25	64 : 25 : 11	-	-	
	Mist	arXiv23	105.93 \pm 9.76	0.83 \pm 0.03	32.48 \pm 1.12	1.24 \pm 0.41	0.11 \pm 0.29	1.02\pm0.11	0.25 \pm 0.28	04 : 06 : 90	98.34	97.23
	Anti-DreamBooth	ICCV23	96.24 \pm 10.44	0.82 \pm 0.03	32.43 \pm 1.10	1.18\pm0.36	0.05 \pm 0.29	1.03 \pm 0.14	0.26 \pm 0.28	03 : 09 : 88	97.38	100.00
	PhotoGuard	ICML23	62.07 \pm 8.15	0.84 \pm 0.03	33.17 \pm 1.21	1.50 \pm 0.54	0.13 \pm 0.34	1.26 \pm 0.30	0.27 \pm 0.31	13 : 19 : 68	98.70	84.02
	SDS(-)	ICLR24	47.48 \pm 6.81	0.81 \pm 0.03	32.91 \pm 0.43	2.09 \pm 0.82	0.07 \pm 0.37	2.74 \pm 0.97	0.33 \pm 0.26	13 : 16 : 71	94.56	77.13
	MetaCloak	CVPR24	204.25 \pm 54.52	0.82 \pm 0.02	32.09 \pm 0.63	1.86 \pm 0.62	0.19 \pm 0.33	1.33 \pm 0.41	0.25 \pm 0.32	02 : 10 : 88	91.03	90.44
	VCPro		27.04\pm4.38	0.90\pm0.03	35.33\pm1.79	2.31 \pm 0.78	0.03\pm0.32	2.06 \pm 0.70	0.21\pm0.34	-	98.61	97.35
CelebA-HQ	No Defense	-	-	-	4.40 \pm 0.86	0.41 \pm 0.22	4.84 \pm 0.40	0.63 \pm 0.13	77 : 19 : 04	-	-	
	Mist	arXiv23	78.32 \pm 11.83	0.86 \pm 0.03	33.75 \pm 0.21	1.45\pm0.58	0.26 \pm 0.26	1.04\pm0.11	0.44 \pm 0.21	05 : 04 : 91	96.29	99.99
	Anti-DreamBooth	ICCV23	78.45 \pm 11.66	0.86 \pm 0.03	33.74 \pm 0.21	1.81 \pm 1.20	0.28 \pm 0.25	1.04 \pm 0.15	0.44 \pm 0.21	00 : 04 : 96	97.01	96.53
	PhotoGuard	ICML23	45.18 \pm 7.21	0.88 \pm 0.02	35.08 \pm 0.25	1.81 \pm 0.59	0.30 \pm 0.24	1.23 \pm 0.35	0.48 \pm 0.17	02 : 22 : 76	94.25	94.31
	SDS(-)	ICLR24	34.53 \pm 6.16	0.82 \pm 0.03	33.01 \pm 0.28	2.29 \pm 0.70	0.09 \pm 0.28	2.92 \pm 0.74	0.55 \pm 0.15	09 : 11 : 80	98.63	84.32
	MetaCloak	CVPR24	161.93 \pm 26.93	0.86 \pm 0.03	33.12 \pm 0.20	1.47 \pm 0.56	0.25 \pm 0.26	1.59 \pm 0.53	0.44 \pm 0.16	00 : 04 : 96	96.02	95.48
	VCPro		16.21\pm2.89	0.95\pm0.01	39.32\pm0.40	2.61 \pm 1.00	0.09\pm0.28	2.62 \pm 0.95	0.44\pm0.19	-	100.00	95.67

For visibility of protected images, we evaluate the average FID/SSIM/PSNR differences between all protected images and their corresponding original images. The statistics show that the protected images generated by our method are more faithful to the original images, and the least variance of FID shows that we also have a stable effect. Compared with our baseline Anti-DreamBooth, we can max reduce 69.20 in FID, up to 0.09 in SSIM, and up to 5.58 in PSNR. Compared with current SOTA methods PhotoGuard and SDS (-), our image quality is still significantly improved. Although SDS (-) achieves a low FID, it introduces noticeable brightness increases in the perturbations, leading to poor SSIM performance.

Protected images against unauthorized AI generation by improving training costs and reducing final AI-generated image quality. For final protection effectiveness, we still have significant relative decreases in full-image quality metric LIQE compared to the no defense (from "good/perfect" to "poor"), again achieving a protective effect, which is similarly confirmed by the manual evaluation later on human evaluation and qualitative results. Considering that the full-image quality metric is not fairly for us, we also add a face region quality metric CLIP-FACE. In CLIP-FACE, we achieve the best protection in most cases. Both metrics demonstrate that we have reduced visibility against perturbations while still having a strong protection effect.

Qualitative Results. Fig. 3 illustrates protected images and protective effects on individual identity information and landscapes of different methods under Textual Inversion and DreamBooth. We also visualize adversarial perturbations by regularizing all perturbations to the range [0,1] and then visualizing using a specific colormap.

Under the protection of our method, the personalization methods fail to generate visual-fidelity results. As shown in the case of important information such as faces, landmark landscapes, or buildings, our adversarial perturbation is less noticeable, especially in the background, and effectively distorts textures and features in crucial areas. This prevents the unauthorized use of personal identification information or copyrighted material, making the perturbation more sub-

tle while still serving its protective purpose. This approach strikes a better balance between safeguarding the content and maintaining its quality, thereby reducing user concerns about image degradation after protection. PhotoGuard, Mist, Anti-DreamBooth, and MetaCloak tend to add strange textures to the whole image and show obvious adversarial perturbations (the second, third, fourth, and sixth columns). SDS(-) can cause generated images to be too blurry and has limited protection for the DreamBooth. Its protected image is like adding strange circular blobs to the original image (the fifth column). Visualization of its perturbations also supports the idea that excessive brightness leads to lower SSIM values. These approaches serve as a protective measure, ensuring that certain image regions exhibit unique textures. The presence of such textures can strongly suggest infringement. We also find that the protection difficulty of Textual Inversion is far less than that of DreamBooth because DreamBooth usually fine-tunes most parameters in Stable Diffusion. At the same time, Textual Inversion only adds a few new word embeddings. It is also supported in Table I.

User Study. We evaluate the performance of VCPro in the concept protection task with five selected methods, i.e., PhotoGuard [12], Mist [14], Anti-DreamBooth [8], SDS(-) [11], and MetaCloak [10]. A total of 50 participants took part in the survey, and they all use social media proficiently. Participants comprise 58% male and 42% female, with ages ranging from 18 to 55 years (mean: 24.5). All participants have normal color vision and social media proficiency relevant to our image protection context. Educational backgrounds span from undergraduate to doctoral level (undergraduate: 54% graduate: 26%, doctoral: 4%). Professional expertise was distributed across computer science (50%), electronic information technology (36%), and visual arts (14%). For quality control, all participants completed preliminary training and visual acuity testing. We implemented consistency checks through randomized question repetition with shuffled options, requiring participants to maintain at least 95% response consistency for inclusion in the final analysis.

We randomly sampled protected images and generated

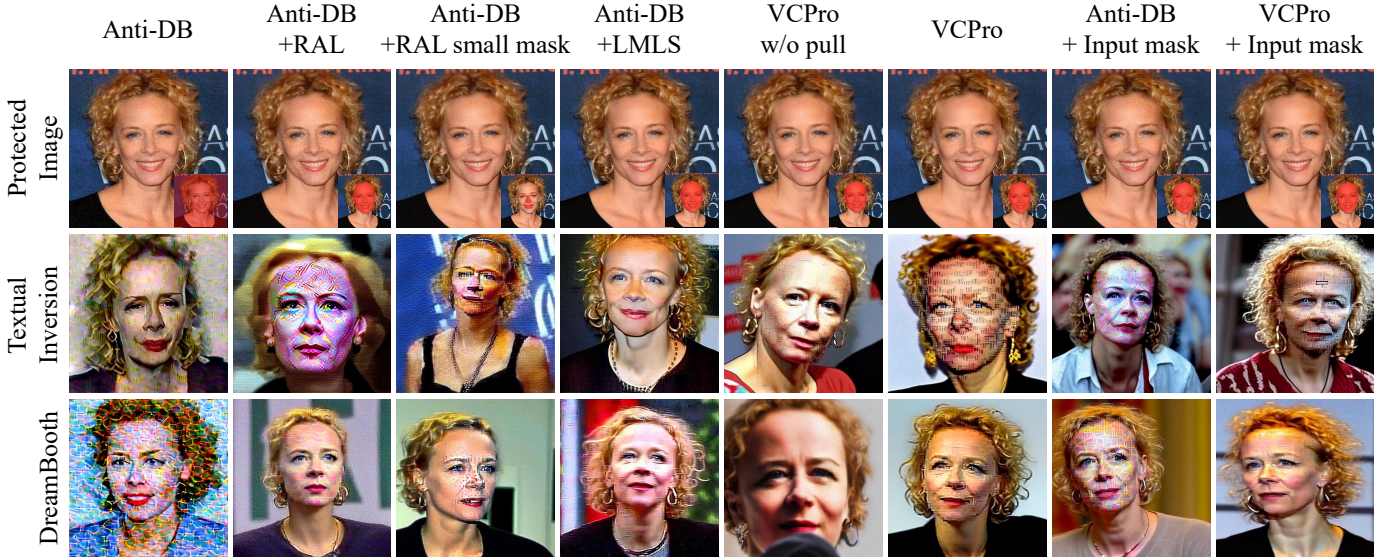


Fig. 4. The ablation experiments of different mask sizes and modules. Anti-DreamBooth (Anti-DB) is our baseline. The red region indicates the important region. Here Input-mask means optimizing adversarial perturbations by directly restricting the mask range. Zoom in for a better view.

images from all 100 identities in VGGFace2 and CelebA-HQ and six groups of non-face data. The study consists of three parts, including visibility of adversarial perturbations (2064 valid votes), protection effects under Textual Inversion (1996 valid votes), and protection effects under DreamBooth (1990 valid votes).

User Study I. In the survey on the visibility of adversarial perturbations, participants were shown a VCPro-protected image alongside a protected image generated by another method based on the same original image. They were then asked to vote on the visual quality, choosing between “A wins”, “tie”, or “B wins”. The visual quality of VCPro was significantly better than that of other methods. As shown in Table I, our VCPro significantly outperformed all baseline methods in direct comparisons. VCPro received between 68% and 96% of participant votes when compared against competing methods. To assess the reliability of our user study results, we calculated the Kendall coefficient [41] as 0.71 ($p < 0.05$), indicating substantial inter-rater agreement among participants.

User Study II. In the survey on protection efficacy under Textual Inversion, participants were given an original image x and asked to determine whether the image generated through Textual Inversion, trained on protected image x' from different methods, was synthetic. As shown in Table I, all protection methods received at least 91% of synthetic votes, with VCPro demonstrating the most effective protection as acknowledged by the majority of participants. To evaluate the consistency of the user study, we calculated Cohen’s Kappa [42], which yielded a value of 0.88 ($p < 0.05$), indicating a strong agreement among participants.

User Study III. In the survey on protection efficacy under DreamBooth, as shown in Table 1, participants recognized an average 97.01% protective success rate of VCPro. To measure the consistency of the study, we calculated Cohen’s Kappa, which resulted in a value of 0.88 ($p < 0.05$).

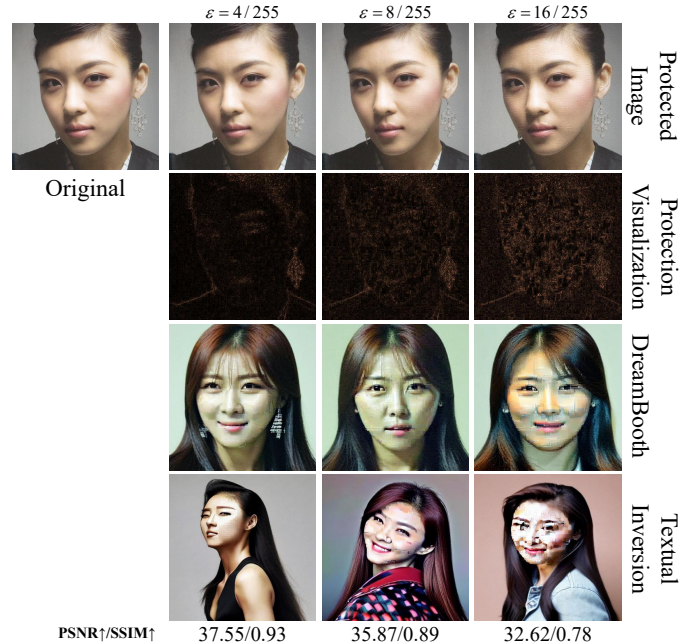


Fig. 5. The influence of different ϵ in VCPro. Numbers under images show the [PSNR \uparrow , SSIM \uparrow] of each generated protected image. Zoom in for a better view.

C. Ablation Study

As shown in Fig. 4 and Table II, we conducted ablation experiments of two modules in VCPro: Regional Adversarial Loss (RAL) in Sec. IV-B and Lagrangian Multiplier-based Loose Solution (LMLS) in Sec. IV-C. Anti-DreamBooth is our baseline.

Compared with Anti-DreamBooth, we find that Anti-DreamBooth+RAL reduces the visibility of the perturbations, while the protection effect is concentrated in the mask area, resulting in a slight decrease in the global image quality assessment LIQE but stable in CLIP-FACE. At the same time, we also consider the effect of different mask ranges, smaller

TABLE II

AUTOMATIC EVALUATION RESULTS ON ABLATION EXPERIMENTS WITH THE CORRESPONDING MEAN AND STANDARD DEVIATION (\pm). ALL METHODS USE $\epsilon = 8/255$ ON VGGFACE2 DATASET. \uparrow MEANS THE HIGHER THE BETTER, AND VICE VERSA. THE BEST RESULT IN EACH COLUMN IS IN BOLD. HERE INPUT-MASK IS TO CONSTRAIN THE ADVERSARIAL PERTURBATIONS DIRECTLY ON THE INPUT IMAGE TO BE ONLY WITHIN THE MASK, WE ARE CONSTRAINING ON THE OPTIMIZATION OBJECTIVE, AND THE ADVERSARIAL PERTURBATIONS WILL BE PRESENT IN THE WHOLE IMAGE.

Methods	Visibility of Perturbations			Textual Inversion		DreamBooth	
	FID \downarrow	SSIM \uparrow	PSNR \uparrow	LIQE \downarrow	CLIP-FACE \downarrow	LIQE \downarrow	CLIP-FACE \downarrow
No Defense	-	-	-	3.61 \pm 0.98	0.24 \pm 0.34	3.95 \pm 1.11	0.38 \pm 0.25
Anti-DreamBooth	96.24 \pm 10.44	0.82 \pm 0.03	32.43 \pm 1.10	1.18\pm0.36	0.05 \pm 0.29	1.03\pm0.14	0.26 \pm 0.28
Anti-DreamBooth+RAL	68.18 \pm 8.58	0.83 \pm 0.03	32.89 \pm 1.25	1.62 \pm 0.57	0.03 \pm 0.31	1.53 \pm 0.53	0.18 \pm 0.31
Anti-DreamBooth+RAL (Small Mask)	58.44 \pm 9.34	0.84 \pm 0.03	33.09 \pm 1.27	2.11 \pm 0.82	0.05 \pm 0.33	2.21 \pm 0.66	0.27 \pm 0.32
Anti-DreamBooth+LMLS	30.08 \pm 5.22	0.90 \pm 0.03	35.03 \pm 1.83	2.52 \pm 0.82	0.17 \pm 0.34	2.16 \pm 0.65	0.30 \pm 0.30
VCPro (w/o Pull)	17.21\pm3.13	0.94\pm0.03	36.79\pm2.34	2.74 \pm 0.82	0.14 \pm 0.33	2.55 \pm 0.92	0.35 \pm 0.32
VCPro	27.04 \pm 4.38	0.90 \pm 0.03	35.33 \pm 1.79	2.31 \pm 0.78	0.03\pm0.32	2.06 \pm 0.70	0.21\pm0.34
Anti-DreamBooth+Input-Mask	41.27 \pm 8.76	0.90 \pm 0.03	35.15 \pm 2.02	2.05 \pm 0.76	0.10 \pm 0.32	2.03 \pm 0.80	0.23 \pm 0.33
VCPro+Input-Mask	18.61 \pm 3.19	0.93 \pm 0.03	36.61 \pm 2.25	2.41 \pm 0.78	0.07 \pm 0.34	2.68 \pm 1.05	0.31 \pm 0.32

masks will further reduce the visibility of the perturbations, and the protection range is further reduced.

LMLS shows a similar phenomenon where Anti-DreamBooth+LMLS reduces the visibility of the noise and tends to leave the high-frequency part, while the final protection effect also leaves a streaky texture across the whole image. Consequently, the adversarial perturbation added to a specific space and frequency domain will directly affect the protection effect in the corresponding space and frequency domains.

Moreover, only push-loss without pull-loss in RAL (VCPro (w/o Pull) in Fig. 4 and Table II) will reduce the training loss gradient feedback about the protection effect, while the loss that constrains the visibility of the perturbations is not affected resulting in decreased visibility of the perturbations and the protection effect.

We also compare the difference between directly protected images updated within the mask range (Input-Mask) and us adding guidance at the loss side, both can achieve the protection of the specified region. When adding the mask constraint directly at the protected images, it improves pixel-level global metrics such as SSIM/PSNR. However, it makes the noise of the protected target on the original image more obvious than us and FID is still high. We can achieve a better visual perception by combining the two, and at the same time, achieve the protection of the target.

D. Perturbation Size Influence

Perturbation size ϵ controls the maximum allowable change in pixel values of adversarial perturbation. As shown in Fig. 5 and Table III, different levels of adversarial perturbation size noticeably influence the protection outcomes: Compared to low ϵ , large ϵ presents worse invisibility of adversarial perturbations while the more obvious protection effects.

For Textual Inversion, when the perturbation size is low, the image preserves the facial area with alterations in facial texture and feature distribution. Upon reaching a perturbation size of 16/255, the facial areas experience complete degradation. The results under DreamBooth and quantitative experiment show a similar trend. Compared with DreamBooth, Textual Inversion is easier to achieve concept protection.

We visualize adversarial perturbations by normalizing all perturbations to the range [0,1] and applying a colormap. An interesting pattern emerges: as ϵ increases, perturbations spread from the face to the background. This diffusion occurs because, when perturbation size is constrained, the perturbations are concentrated in areas that most effectively enhance the protective effect.

E. Hyper-parameter Analysis

Here we provide quantitative results to study the influence of hyper-parameters: training iteration, c , and α . We also provide qualitative results in supplementary materials.

Sensitivity Analysis of Training Iteration. Usually, the larger the training steps, the larger the value of \mathcal{L}'_{θ} at different time steps, and the more successful the protection is. As shown in Fig. 14 (a), when increasing the number of training iterations, FID will first improve rapidly and then rise slowly, and the overall trend is that the longer the training iterations, the worse the quality of the protected image. Whereas LIQE will fall rapidly and then level off, the protection effect will improve and then keep stable. Finally, we selected 720 iterations based on the inflection point observed in Fig. 14 (a). At this point, we achieve substantial protection effectiveness (LIQE-SUM 4.37) while maintaining reasonable image quality (FID 27.04). Increasing iterations beyond 720 provides only marginal improvements in protection while continuing to degrade image quality.

Sensitivity Analysis of c . c represents stronger constraints on perturbation visibility. As shown in Fig. 14 (b), increasing parameter c reduces the FID score from 68.18 at $c = 0.0$ to 15.33 at $c = 1.0$, indicating significant improvements in visual quality of protected images. Meanwhile, protection effectiveness (LIQE-SUM) increases from 3.15 at $c = 0.0$ to 5.43 at $c = 0.5$, then slightly decreases to 4.75 at $c = 1.0$. Based on the analysis, we selected $c = 0.1$ as the optimal value, balancing acceptable protection effectiveness with maintainable visual quality.

Sensitivity Analysis of Parameter α . Fig. 17 (a) illustrates the impact of α on visual quality and protection effectiveness. Increasing α from 0 to 0.005 sharply increases FID from 0 to 33.93 (indicating more noticeable perturbations)

TABLE III

THE INFLUENCE OF DIFFERENT PERTURBATION SIZE ϵ ON VGGFACE2 DATASETS. \uparrow MEANS THE HIGHER THE BETTER, AND VICE VERSA. THE BEST RESULT IN EACH COLUMN IS IN BOLD.

Budget	Visibility of Perturbations			Textual Inversion		DreamBooth	
	FID \downarrow	SSIM \uparrow	PSNR \uparrow	LIQE \downarrow	CLIP-FACE \downarrow	LIQE \downarrow	CLIP-FACE \downarrow
0	-	-	-	3.61 ± 0.98	0.24 ± 0.34	3.95 ± 1.11	0.38 ± 0.25
4	22.98 ± 4.08	0.93 ± 0.03	36.45 ± 2.21	2.76 ± 0.77	-0.02 ± 0.27	2.33 ± 0.70	0.25 ± 0.31
8	27.04 ± 4.38	0.90 ± 0.03	35.33 ± 1.79	2.31 ± 0.78	0.03 ± 0.32	2.06 ± 0.70	0.21 ± 0.34
16	48.67 ± 9.02	0.82 ± 0.03	32.63 ± 1.06	1.86 ± 0.80	-0.02 ± 0.23	1.81 ± 0.53	0.19 ± 0.32

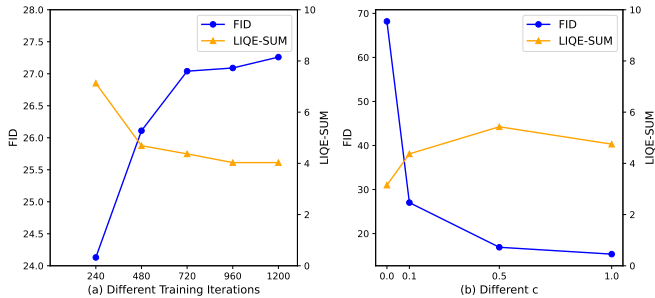


Fig. 6. Sensitivity analysis of hyper-parameters training iterations and c . FID is calculated between adversarial data and corresponding clean data; here LIQE-SUM is the sum LIQE of Textual Inversion and DreamBooth, which are all the smaller the better. The dataset is VGGface2 and $\epsilon = 8/255$.

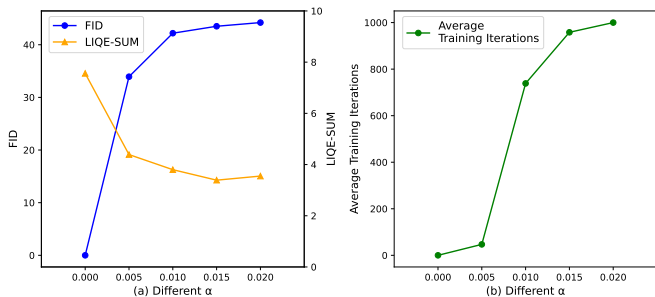


Fig. 7. Sensitivity analysis of hyper-parameter α . FID is calculated between adversarial data and corresponding clean data; here LIQE-SUM is the sum LIQE of Textual Inversion and DreamBooth, which are all the smaller the better. The dataset is VGGFace2 and $\epsilon = 8/255$.

while decreasing LIQE-SUM from 7.56 to 4.39 (indicating enhanced protection). Further increases to $\alpha = 0.020$ continue improving FID to 44.21 but result in saturated protection effectiveness (LIQE-SUM 3.55). Fig. 17 (b) shows that larger α values (e.g., 0.015, 0.020) require significantly more training iterations (1000) to converge compared to smaller values (e.g., $\alpha = 0.005$ requiring 80 iterations). We set $\alpha = 0.005$, which balances among visual quality, protection effectiveness, and computational efficiency.

Note that Fig. 17 uses $c = 0.005$ to clearly demonstrate the relationship between α and training iterations, as α values at $c = 0.1$ remain around 0.005 across the 240-1200 iteration range, making visualization challenging. In practice, we adjust training steps to facilitate parallel acceleration to influence α .

F. Analysis of Adversary Settings

Following Anti-DreamBooth [8], we consider three settings in this paper: “convenient setting”, “adverse setting”, and



Fig. 8. Experiments about different adversarial settings. Protector uses Stable Diffusion v1-4. Zoom in for a better view.

TABLE IV

RESULTS OF MODEL MISMATCHING SETTING WITH THE CORRESPONDING MEAN AND STANDARD DEVIATION (\pm). \uparrow DENOTES THAT HIGHER VALUES ARE PREFERABLE, WHILE \downarrow INDICATES THE OPPOSITE. THE BEST RESULT IN EACH COLUMN IS HIGHLIGHTED IN BOLD. SD IS SHORT FOR STABLE DIFFUSION.

Protector	Adversary	Textual Inversion		DreamBooth	
		LIQE \downarrow	CLIP-FACE \downarrow	LIQE \downarrow	CLIP-FACE \downarrow
No Defense	SD v1-4	3.61 ± 0.98	0.24 ± 0.34	3.95 ± 1.11	0.38 ± 0.25
SD v1-4	SD v1-4	2.31 ± 0.78	0.03 ± 0.32	2.06 ± 0.70	0.21 ± 0.34
SD v1-4	SD v1-5	2.06 ± 0.74	0.02 ± 0.32	2.00 ± 0.57	0.24 ± 0.34
SD v1-4	SD v2-1 base	1.82 ± 0.60	0.06 ± 0.30	1.70 ± 0.49	0.20 ± 0.34

“uncontrolled setting”.

Convenient Setting. In a convenient setting (white-box setting), we (protectors) have all knowledge of the resources of adversary, including a pre-trained text-to-image generator, training term (e.g., “sks”), and training prompt. This scenario is practical because adversaries are likely to use high-quality, open-source pre-trained generators, with Stable Diffusion being the most prominent publicly available model. Additionally, people often rely on open-source code with default training terms and prompts. The convenient setting is the simplest for the protectors, and all relevant experiment results have been analyzed and mentioned in Sec. V-B.

Adverse Settings. In adverse settings, also known as grey-box settings, protectors lack knowledge of the specific version of the pre-trained text-to-image generator, training term, or training prompt employed by the adversary. This scenario more closely resembles real-world conditions. To

TABLE V

RESULTS OF TRAINING TERM MISMATCHING SETTING WITH THE CORRESPONDING MEAN AND STANDARD DEVIATION (\pm). \uparrow MEANS THE HIGHER THE BETTER, AND VICE VERSA. THE BEST RESULT IN EACH COLUMN IS IN BOLD.

Protector	Adversary	Textual Inversion		DreamBooth	
		LIQE \downarrow	CLIP-FACE \downarrow	LIQE \downarrow	CLIP-FACE \downarrow
No Defense	sks	3.61 ± 0.98	0.24 ± 0.34	3.95 ± 1.11	0.38 ± 0.25
sks	sks	2.31 ± 0.78	0.03 ± 0.32	2.06 ± 0.70	0.21 ± 0.34
sks	t@t	2.03 ± 0.74	0.04 ± 0.34	1.93 ± 0.66	0.21 ± 0.33

TABLE VI

RESULTS OF TRAINING PROMPT MISMATCHING SETTING WITH THE CORRESPONDING MEAN AND STANDARD DEVIATION (\pm). \uparrow MEANS THE HIGHER THE BETTER, AND VICE VERSA. THE BEST RESULT IN EACH COLUMN IS IN BOLD.

Protector	Adversary	Textual Inversion		DreamBooth	
		LIQE \downarrow	CLIP-FACE \downarrow	LIQE \downarrow	CLIP-FACE \downarrow
No Defense	“a photo of sks person.”	3.61 \pm 0.98	0.24 \pm 0.34	3.95 \pm 1.11	0.38 \pm 0.25
“a photo of sks person.”	“a photo of sks person.”	2.31 \pm 0.78	0.03\pm0.32	2.06\pm0.70	0.21\pm0.34
“a photo of sks person.”	“a dslr portrait of sks person.”	2.23\pm0.77	0.04 \pm 0.32	2.62 \pm 1.18	0.22 \pm 0.32

TABLE VII

RESULTS OF DIFFERENT POST-PROCESSING WITH THE CORRESPONDING MEAN AND STANDARD DEVIATION (\pm). \uparrow MEANS THE HIGHER THE BETTER, AND VICE VERSA. THE BEST RESULT IN EACH COLUMN IS IN BOLD.

Protector	Adversary	Textual Inversion		DreamBooth	
		LIQE \downarrow	CLIP-FACE \downarrow	LIQE \downarrow	CLIP-FACE \downarrow
No Defense	Null	3.61 \pm 0.98	0.24 \pm 0.34	3.95 \pm 1.11	0.38 \pm 0.25
Null	Null	2.31 \pm 0.78	0.03\pm0.32	2.06\pm0.70	0.21\pm0.34
Null	Gaussian Filtering	2.56 \pm 0.78	0.18 \pm 0.31	2.18 \pm 0.44	0.31 \pm 0.34
Null	JPEG Compression	2.08\pm0.79	0.12 \pm 0.33	2.09 \pm 0.46	0.29 \pm 0.32

TABLE VIII

RESULTS OF DIFFERENT UNCONTROLLED SETTINGS WITH THE CORRESPONDING MEAN AND STANDARD DEVIATION (\pm). \uparrow MEANS THE HIGHER THE BETTER, AND VICE VERSA. THE BEST RESULT IN EACH COLUMN IS IN BOLD.

Perturbed	Clean	Textual Inversion		DreamBooth	
		LIQE \downarrow	CLIP-FACE \downarrow	LIQE \downarrow	CLIP-FACE \downarrow
0	100%	3.61 \pm 0.98	0.24 \pm 0.34	3.95 \pm 1.11	0.38 \pm 0.25
25%	75%	2.82 \pm 1.12	0.20 \pm 0.34	3.50 \pm 1.25	0.40 \pm 0.28
50%	50%	2.15 \pm 0.81	0.05 \pm 0.35	2.89 \pm 1.21	0.35 \pm 0.32
75%	25%	2.03\pm0.74	0.04 \pm 0.34	2.71 \pm 1.07	0.33 \pm 0.32
100%	0%	2.31 \pm 0.78	0.03\pm0.32	2.06\pm0.70	0.21\pm0.34

defend against such attacks, protectors typically use surrogate modules to test the transferability of adversarial perturbations. Experiments under both assumptions demonstrate the practicality of our method in real-world scenarios. All experiments utilize $\epsilon = 8/255$ as the perturbation size on the VGGFace2 dataset, with Stable Diffusion v1-4 as the base model, except in the case of model mismatching.

- **Model Mismatching.** In this scenario, protectors use Stable Diffusion v1-4 without knowing the specific version of Stable Diffusion employed by the adversary. Results in Fig. 8 and Table IV show effective facial area protection even if adversaries used Stable Diffusion v1-4/v1-5/v2-1, which reflects the transferability of VCPro.
- **Training Term Mismatching.** We set protectors to use “sks” as a training term in Textual Inversion and DreamBooth, and adversaries use “t@t”. As shown in Fig. 8 and Table V, VCPro is robust to different training terms.
- **Training Prompt Mismatching.** We set protectors to use “a photo of sks person.” as training prompt in Textual Inversion and DreamBooth, and adversaries to use “a dslr portrait of sks person.”. As shown in Fig. 8 and Table VI, VCPro can still successfully protect the important concepts.
- **Post-Processing.** In this setting, we assume that the adversaries will use some post-processing to reduce the impact of the protected images, taking the two common post-processing techniques, Gaussian filtering and JPEG compression, as an example. Here we set the kernel

size 7×7 for Gaussian filtering and adopt 75% quality compression for JPEG, which also mentioned in [43] can be a good purification method. As shown in Fig. 8 and Table VII, although the protective effect is somewhat diminished, the final generated image is still visibly cracked. VCPro can still successfully protect the target area.

Uncontrolled Settings. In this section, we examine the scenario where an adversary has access to a set of original images of the target concept, which are then combined with protected images to train DreamBooth. We evaluate three settings in which the proportion of original images is varied from 25% to 75%, as detailed in Table VIII. All experiments employ a perturbation size of $\epsilon = 8/255$ on the VGGFace2 dataset and utilize Stable Diffusion v1-4 as the base model. Our protection remains effective as long as the proportion of protected images exceeds 50%, but its effectiveness diminishes as the proportion of original images increases. Ideally, VCPro would receive platform support, become widely adopted, and be implemented across all social media platforms, thereby mitigating the risks associated with these uncontrolled settings.

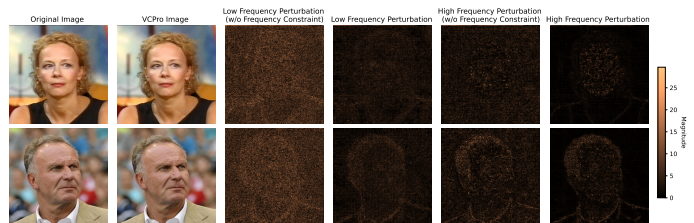


Fig. 9. Frequency domain visualization of perturbations. From left to right: (1) Original image, (2) VCPro protected image, (3) Perturbation without our frequency constraint in low-frequency, (4) Perturbation with our frequency constraint in low-frequency, (5) Perturbation without our frequency constraint in high-frequency, (6) Perturbation with our frequency constraint in high-frequency. The color bar indicates the magnitude of perturbation.

TABLE IX

RESULTS OF FREQUENCY ANALYSIS. THE DATASET IS VGGFACE2, AND THE PERTURBATION SIZE IS $8/255$. \uparrow DENOTES THAT HIGHER VALUES ARE PREFERABLE, WHILE \downarrow INDICATES THE OPPOSITE. AVERAGE LOW/HIGH FREQUENCY DIFFERENCE IS CALCULATED BASED ON THE AVERAGE L1 NORM PER PIXEL. THE BEST RESULT IN EACH COLUMN IS HIGHLIGHTED IN BOLD.

Metric	VCPro	w/o Freq. Constr.
Avg. Low Freq. Diff. (\downarrow)	6.80	17.39
Avg. High Freq. Diff. (\downarrow)	6.98	11.47
Low Freq. Ratio (%) (\downarrow)	49.37	60.26
High Freq. Ratio (%) (\uparrow)	50.63	39.74

G. Frequency Domain Analysis

We analyzed the frequency characteristics of VCPro via

Discrete Wavelet Transform (DWT) with Haar wavelet decomposition, consistent with our perturbation generation process. This analysis is significant as human visual perception exhibits more sensitivity in low-frequency components than in high-frequency details. We compared two variants: VCPro with frequency constraint, and without frequency constraint where $D(\cdot) = \|x - x'\|_2^2$ in Eq. 8. Further implementation details are provided in the supplementary materials.

Visualization in Different Frequency Components. Fig. 9 shows the frequency visualization of sample images. The frequency-constrained variant shows significantly attenuated low-frequency perturbations (column 4) compared to the unconstrained variant (column 3); and concentrates perturbations predominantly in high-frequency components (column 6), with perturbation patterns that correspond to facial contours and edge features. Conversely, the unconstrained variant exhibits perturbation distribution across both frequency domains, with notably higher concentration in visually sensitive low-frequency regions (columns 3 and 5). Despite the protective modifications, the perceptual difference between original and protected images remains minimal.

Statistical Analysis in Different Frequency Components. Table IX provides a statistical analysis to quantify the frequency distribution of perturbations using the VGGFace2 dataset. With our frequency constraint, both low-frequency (6.80) and high-frequency (6.98) differences are substantially lower than without the constraint (17.39 and 11.47, respectively). Meanwhile, the frequency constraint effectively shifts perturbation distribution, reducing low-frequency components from 60.26% (unconstrained) to 49.37% (constrained). Both findings effectively explain the improved visual quality of the constrained approach as low-frequency perturbations are more perceptible to human vision.

VI. CONCLUSION

In this paper, we show that existing approaches utilizing adversarial perturbations to safeguard images from malicious personalization often overemphasize the final protection effectiveness, resulting in more noticeable perturbations. To mitigate this problem, on the one hand, we protect the important concept regions rather than the full images in previous works, leveraging the sparse nature of images and designing a user-specified image concepts protection framework. On the other hand, we change the optimization objective from generating the most protective adversarial perturbation to generating the least perceptible adversarial perturbation that exactly achieves the required protective effect. Quantitative and qualitative experiments demonstrate that we can protect important user-specified concepts and greatly reduce the degree of naked-eye visibility of adversarial perturbations.

Future Works and Limitations. We have not yet reached the capability to generate protected images in real time. However, we are committed to ongoing research and development in this area. Our future efforts will focus on finding efficient methods to produce protected images swiftly while maintaining high visual quality. By doing so, we aim to significantly enhance the overall user experience and ensure that

our solutions meet the highest standards of both functionality and aesthetics.

ACKNOWLEDGMENTS

We would like to express our gratitude to Yu Wu for his valuable discussions and support during the early stages of the experiments. Thanks are also due to Zijun Zhou for developing the user study system, and to Xiaoyu Kong for his assistance in the aesthetic aspects of the figures.

REFERENCES

- [1] J. Ho, A. Jain, and P. Abbeel, "Denoising diffusion probabilistic models," *Advances in neural information processing systems*, vol. 33, pp. 6840–6851, 2020.
- [2] R. Rombach, A. Blattmann, D. Lorenz, P. Esser, and B. Ommer, "High-resolution image synthesis with latent diffusion models," in *Proceedings of the IEEE/CVF conference on computer vision and pattern recognition*. IEEE, 2022, pp. 10 684–10 695.
- [3] J. Song, C. Meng, and S. Ermon, "Denoising diffusion implicit models," *arXiv preprint arXiv:2010.02502*, 2020.
- [4] J. Achiam, S. Adler, S. Agarwal, L. Ahmad, I. Akkaya, F. L. Aleman, D. Almeida, J. Altschmidt, S. Altman, S. Anadkat *et al.*, "Gpt-4 technical report," *arXiv preprint arXiv:2303.08774*, 2023.
- [5] X. Luo, Y. Jiang, F. Wei, Y. Wu, X. Xiao, and B. C. Ooi, "Exploring privacy and fairness risks in sharing diffusion models: An adversarial perspective," *IEEE Transactions on Information Forensics and Security*, 2024.
- [6] R. Gal, Y. Alaluf, Y. Atzmon, O. Patashnik, A. H. Bermano, G. Chechik, and D. Cohen-or, "An image is worth one word: Personalizing text-to-image generation using textual inversion," in *The Eleventh International Conference on Learning Representations*, 2022.
- [7] N. Ruiz, Y. Li, V. Jampani, Y. Pritch, M. Rubinstein, and K. Aberman, "Dreambooth: Fine tuning text-to-image diffusion models for subject-driven generation," in *Proceedings of the IEEE/CVF Conference on Computer Vision and Pattern Recognition*. IEEE, 2023, pp. 22 500–22 510.
- [8] T. V. Le, H. Phung, T. H. Nguyen, Q. Dao, N. Tran, and A. Tran, "Anti-dreambooth: Protecting users from personalized text-to-image synthesis," in *Proceedings of the IEEE/CVF International Conference on Computer Vision (ICCV)*. IEEE, 2023, pp. 2116–2127.
- [9] J. Zhang, B. Li, J. Xu, S. Wu, S. Ding, L. Zhang, and C. Wu, "Towards efficient data free black-box adversarial attack," in *Proceedings of the IEEE/CVF Conference on Computer Vision and Pattern Recognition*. IEEE, 2022, pp. 15 115–15 125.
- [10] Y. Liu, C. Fan, Y. Dai, X. Chen, P. Zhou, and L. Sun, "Metacloak: Preventing unauthorized subject-driven text-to-image diffusion-based synthesis via meta-learning," in *Proceedings of the IEEE/CVF Conference on Computer Vision and Pattern Recognition*, 2024, pp. 24 219–24 228.
- [11] H. Xue, C. Liang, X. Wu, and Y. Chen, "Toward effective protection against diffusion-based mimicry through score distillation," in *The Twelfth International Conference on Learning Representations*, 2024.
- [12] H. Salman, A. Khaddaj, G. Leclerc, A. Ilyas, and A. Madry, "Raising the cost of malicious ai-powered image editing," *arXiv preprint arXiv:2302.06588*, 2023.
- [13] C. Liang, X. Wu, Y. Hua, J. Zhang, Y. Xue, T. Song, X. Zhengui, R. Ma, and H. Guan, "Adversarial example does good: Preventing painting imitation from diffusion models via adversarial examples," 2023.
- [14] C. Liang and X. Wu, "Mist: Towards improved adversarial examples for diffusion models," *arXiv preprint arXiv:2305.12683*, 2023.
- [15] S. Shan, J. Cryan, E. Wenger, H. Zheng, R. Hanocka, and B. Y. Zhao, "Glaze: Protecting artists from style mimicry by text-to-image models," 2023.
- [16] A. Voynov, Q. Chu, D. Cohen-Or, and K. Aberman, "p+: Extended textual conditioning in text-to-image generation," *arXiv preprint arXiv:2303.09522*, 2023.
- [17] Y. Zhang, W. Dong, F. Tang, N. Huang, H. Huang, C. Ma, T.-Y. Lee, O. Deussen, and C. Xu, "Prospect: Prompt spectrum for attribute-aware personalization of diffusion models," *ACM Trans. Graph.*, vol. 42, no. 6, dec 2023.

- [18] N. Kumari, B. Zhang, R. Zhang, E. Shechtman, and J.-Y. Zhu, “Multi-concept customization of text-to-image diffusion,” in *Proceedings of the IEEE/CVF Conference on Computer Vision and Pattern Recognition*. IEEE, 2023, pp. 1931–1941.
- [19] C. Szegedy, W. Zaremba, I. Sutskever, J. Bruna, D. Erhan, I. Goodfellow, and R. Fergus, “Intriguing properties of neural networks,” *arXiv preprint arXiv:1312.6199*, 2013.
- [20] N. Carlini and D. Wagner, “Towards evaluating the robustness of neural networks,” in *2017 IEEE symposium on security and privacy*. IEEE, 2017, pp. 39–57.
- [21] R. Duan, Y. Chen, D. Niu, Y. Yang, A. K. Qin, and Y. He, “Advdrop: Adversarial attack to dnns by dropping information,” in *Proceedings of the IEEE/CVF International Conference on Computer Vision*. IEEE, 2021, pp. 7506–7515.
- [22] X. Mi, F. Tang, Z. Yang, D. Wang, J. Cao, P. Li, and Y. Liu, “Adversarial robust memory-based continual learner,” *arXiv preprint arXiv:2311.17608*, 2023.
- [23] R. Zhao, T. Liu, J. Xiao, D. P. Lun, and K.-M. Lam, “Invertible image decolorization,” *IEEE Transactions on Image Processing*, vol. 30, pp. 6081–6095, 2021.
- [24] C. Luo, Q. Lin, W. Xie, B. Wu, J. Xie, and L. Shen, “Frequency-driven imperceptible adversarial attack on semantic similarity,” in *Proceedings of the IEEE/CVF conference on computer vision and pattern recognition*. IEEE, 2022, pp. 15 315–15 324.
- [25] S. Jia, C. Ma, T. Yao, B. Yin, S. Ding, and X. Yang, “Exploring frequency adversarial attacks for face forgery detection,” in *Proceedings of the IEEE/CVF Conference on Computer Vision and Pattern Recognition*. IEEE, 2022, pp. 4103–4112.
- [26] Z. Chen, Z. Wang, J.-J. Huang, W. Zhao, X. Liu, and D. Guan, “Imperceptible adversarial attack via invertible neural networks,” in *Proceedings of the AAAI Conference on Artificial Intelligence*, vol. 37. AAAI Press, 2023, pp. 414–424.
- [27] H. Wu, J. Zhou, J. Tian, J. Liu, and Y. Qiao, “Robust image forgery detection against transmission over online social networks,” *IEEE Transactions on Information Forensics and Security*, vol. 17, pp. 443–456, 2022.
- [28] H. Li, W. Luo, and J. Huang, “Localization of diffusion-based inpainting in digital images,” *IEEE transactions on information forensics and security*, vol. 12, no. 12, pp. 3050–3064, 2017.
- [29] N. Ruiz, S. A. Bargal, and S. Sclaroff, “Disrupting deepfakes: Adversarial attacks against conditional image translation networks and facial manipulation systems,” in *Computer Vision–ECCV 2020 Workshops: Glasgow, UK, August 23–28, 2020, Proceedings, Part IV 16*. Springer, 2020, pp. 236–251.
- [30] R. Wang, Z. Huang, Z. Chen, L. Liu, J. Chen, and L. Wang, “Anti-forgery: Towards a stealthy and robust deepfake disruption attack via adversarial perceptual-aware perturbations,” in *Proceedings of the Thirty-First International Joint Conference on Artificial Intelligence, IJCAI-22*, L. D. Raedt, Ed. International Joint Conferences on Artificial Intelligence Organization, 7 2022, pp. 761–767, main Track.
- [31] X. Wang, J. Huang, S. Ma, S. Nepal, and C. Xu, “Deepfake disrupter: The detector of deepfake is my friend,” in *Proceedings of the IEEE/CVF Conference on Computer Vision and Pattern Recognition*. IEEE, 2022, pp. 14 920–14 929.
- [32] Y. Zhu, Y. Chen, X. Li, R. Zhang, X. Tian, B. Zheng, and Y. Chen, “Information-containing adversarial perturbation for combating facial manipulation systems,” *IEEE Transactions on Information Forensics and Security*, vol. 18, pp. 2046–2059, 2023.
- [33] A. Kirillov, E. Mintun, N. Ravi, H. Mao, C. Rolland, L. Gustafson, T. Xiao, S. Whitehead, A. C. Berg, W.-Y. Lo, P. Dollar, and R. Girshick, “Segment anything,” in *Proceedings of the IEEE/CVF International Conference on Computer Vision (ICCV)*. IEEE, October 2023, pp. 4015–4026.
- [34] T. Karras, T. Aila, S. Laine, and J. Lehtinen, “Progressive growing of gans for improved quality, stability, and variation,” *arXiv preprint arXiv:1710.10196*, 2017.
- [35] Q. Cao, L. Shen, W. Xie, O. M. Parkhi, and A. Zisserman, “Vggface2: A dataset for recognising faces across pose and age,” in *2018 13th IEEE international conference on automatic face & gesture recognition*. IEEE, 2018, pp. 67–74.
- [36] B. Poole, A. Jain, J. T. Barron, and B. Mildenhall, “Dreamfusion: Text-to-3d using 2d diffusion,” *arXiv preprint arXiv:2209.14988*, 2022.
- [37] M. Heusel, H. Ramsauer, T. Unterthiner, B. Nessler, and S. Hochreiter, “Gans trained by a two time-scale update rule converge to a local nash equilibrium,” in *Advances in Neural Information Processing Systems*, I. Guyon, U. V. Luxburg, S. Bengio, H. Wallach, R. Fergus, S. Vishwanathan, and R. Garnett, Eds., vol. 30. Curran Associates, Inc., 2017.
- [38] Z. Wang, A. C. Bovik, H. R. Sheikh, and E. P. Simoncelli, “Image quality assessment: from error visibility to structural similarity,” *IEEE transactions on image processing*, vol. 13, no. 4, pp. 600–612, 2004.
- [39] W. Zhang, G. Zhai, Y. Wei, X. Yang, and K. Ma, “Blind image quality assessment via vision-language correspondence: A multitask learning perspective,” in *Proceedings of the IEEE/CVF Conference on Computer Vision and Pattern Recognition (CVPR)*. Vancouver, BC, Canada: IEEE, June 2023, pp. 14 071–14 081.
- [40] J. Wang, K. C. Chan, and C. C. Loy, “Exploring clip for assessing the look and feel of images,” in *Proceedings of the AAAI Conference on Artificial Intelligence*, vol. 37. AAAI Press, 2023, pp. 2555–2563.
- [41] H. Abdi, “The kendall rank correlation coefficient,” *Encyclopedia of measurement and statistics*, vol. 2, pp. 508–510, 2007.
- [42] J. Cohen, “A coefficient of agreement for nominal scales,” *Educational and psychological measurement*, vol. 20, no. 1, pp. 37–46, 1960.
- [43] P. Sandoval-Segura, J. Geiping, and T. Goldstein, “Jpeg compressed images can bypass protections against ai editing,” *arXiv preprint arXiv:2304.02234*, 2023.



Fig. 13. More qualitative defense results. For generating protected images, we use an ϵ value of $8/255$ with Stable Diffusion v1-4. Each row displays the original images (No Defense), the protected images generated our method, along with respective outcomes in Textual Inversion (TI) and DreamBooth (DB). For better detail, please zoom in.

APPENDIX

We show more cases of VCPro in Fig.13. VCPro can generate visually friendly perturbations while maintaining protection effectiveness.

Here we provide quantitative results to study the influence of hyper-parameters: training iteration, c , and α . We also provide qualitative results in supplementary materials. **Sensitivity Analysis of Training Iteration.** Usually, the larger the training steps, the larger the value of \mathcal{L}'_{θ} at different time steps, and the more successful the protection is. As shown in Fig. 14 (a), when increasing the number of training iterations, FID will first improve rapidly and then rise slowly, and the overall trend is that the longer the training iterations, the worse the quality of the protected image. Whereas LIQE will fall rapidly and then level off, the protection effect will improve and then remain stable. Finally, we selected 720 iterations based on the inflection point observed in Fig. 14 (a). At this point, we achieve substantial protection effectiveness (LIQE-SUM 4.37) while maintaining reasonable image quality (FID 27.04), and Fig. 15 also shows similar pheonmitions. Increasing iterations beyond 720 provides only marginal improvements in protection while continuing to degrade image quality.

Sensitivity Analysis of c . c represents stronger constraints on perturbation visibility. As shown in Fig. 14 (b), increasing parameter c reduces the FID score from 68.18 at $c = 0.0$ to 15.33 at $c = 1.0$, indicating significant improvements in visual quality of protected images. Meanwhile, protection effectiveness (LIQE-SUM) increases from 3.15 at $c = 0.0$ to 5.43 at $c = 0.5$, then slightly decreases to 4.75 at $c = 1.0$. Fig. 16 presents qualitative results across different c values, demonstrating that smaller c values (e.g., $c = 0.0$) provide stronger protection but compromise visual quality, while larger c values (e.g., $c = 1.0$) lead to friendly visibility with reduced

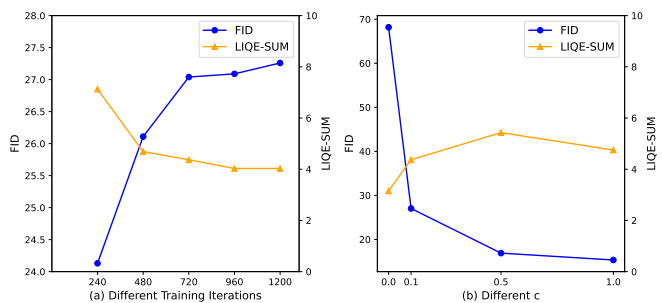


Fig. 14. Sensitivity analysis of hyper-parameters training iterations and c . FID is calculated between adversarial data and corresponding clean data; here LIQE-SUM is the sum LIQE of Textual Inversion and DreamBooth, which are all the smaller the better. The dataset is VGGface2 and $\epsilon = 8/255$.

protection. Based on analysis, we selected $c = 0.1$ as the optimal value, balancing acceptable protection effectiveness with maintainable visual quality.

Sensitivity Analysis of Parameter α . Fig. 17 (a) illustrates the impact of α on visual quality and protection effectiveness. Increasing α from 0 to 0.005 sharply increases FID from 0 to 33.93 (indicating more noticeable perturbations) while decreasing LIQE-SUM from 7.56 to 4.39 (indicating enhanced protection). Further increases to $\alpha = 0.020$ continue improving FID to 44.21 but result in saturated protection effectiveness (LIQE-SUM 3.55). Fig. 17 (b) shows that larger α values (e.g., 0.015, 0.020) require significantly more training iterations (1000) to converge compared to smaller values (e.g., $\alpha = 0.005$ requiring 80 iterations). Qualitative results in Fig. 18 show similar trends. We set $\alpha = 0.005$, which balances among visual quality, protection effectiveness, and computational efficiency.

Note that Fig. 17 uses $c = 0.005$ to clearly demonstrate the relationship between α and training iterations, as α values at

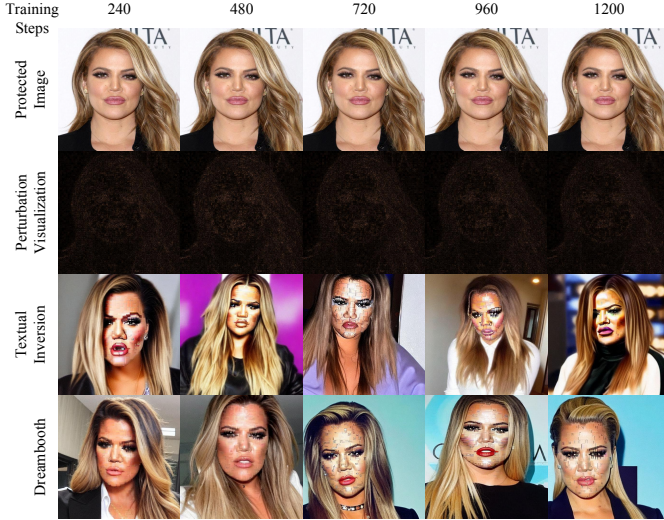


Fig. 15. Qualitative results for different training steps. For generating protected images, we use an ϵ value of $8/255$ with Stable Diffusion v1-4. For better detail, please zoom in.

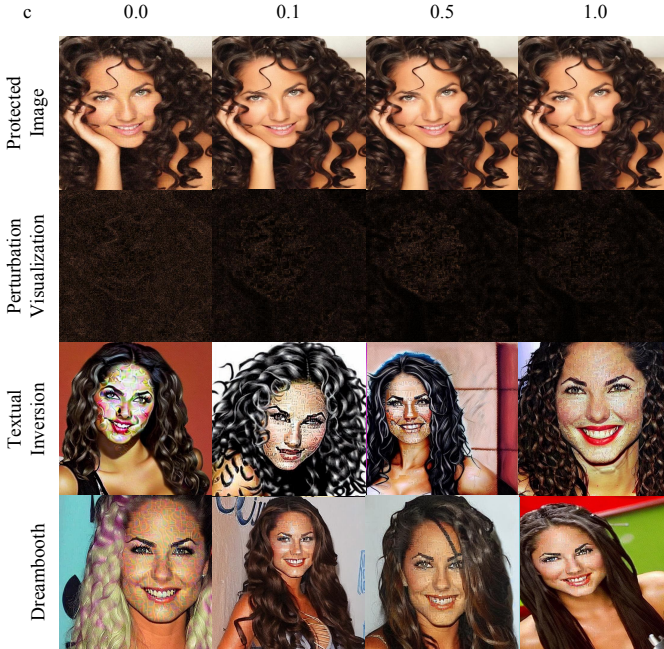


Fig. 16. Qualitative results for different c . For generating protected images, we use an ϵ value of $8/255$ with Stable Diffusion v1-4. For better detail, please zoom in.

$c = 0.1$ remain around 0.005 across the 240-1200 iteration range, making visualization challenging. In practice, to facilitate parallel acceleration, we adjust training steps to influence α . For each RGB image I , we performed the following analysis:

- 1) Apply 2D DWT to each color channel $c \in \{R, G, B\}$ separately:

$$\text{DWT}_c = \text{dwt2}(I_c, \text{'haar'})$$

- 2) Extract the approximation coefficients (low-frequency component) cA_c and detail coefficients (high-frequency components) cH_c , cV_c , and cD_c :

$$\text{DWT}_c = (cA_c, (cH_c, cV_c, cD_c))$$

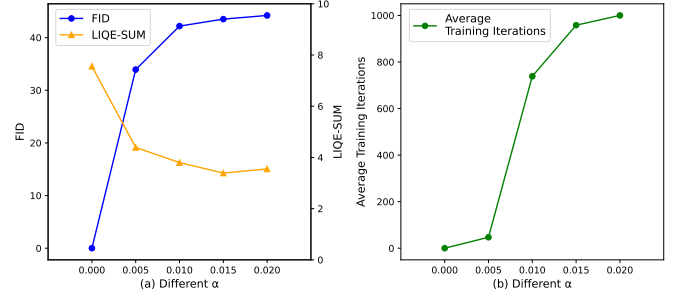


Fig. 17. Sensitivity analysis of hyper-parameter α . FID is calculated between adversarial data and corresponding clean data; here LIQE-SUM is the sum LIQE of Textual Inversion and DreamBooth, which are all the smaller the better. The dataset is VGGFace2 and $\epsilon = 8/255$.

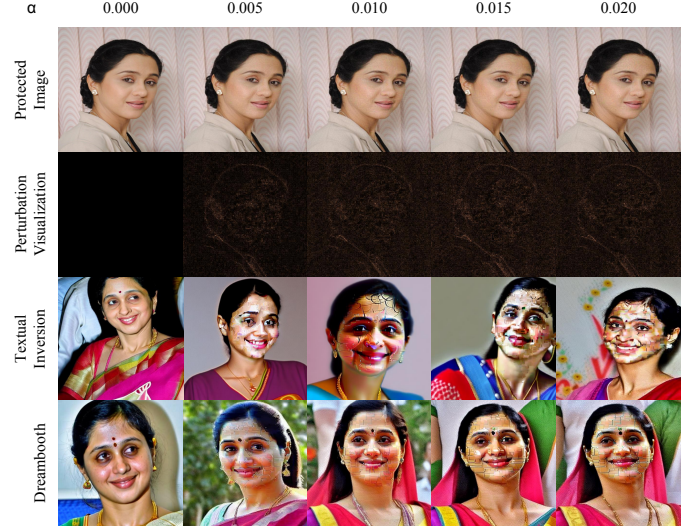


Fig. 18. Qualitative results for different α . For generating protected images, we use an ϵ value of $8/255$ with Stable Diffusion v1-4. For better detail, please zoom in.

- 3) Compute the combined high-frequency magnitude for each channel:

$$H_c = \sqrt{cH_c^2 + cV_c^2 + cD_c^2}$$

- 4) Calculate the frequency differences between clean image I and protected image I' :

- Low-frequency difference: $\Delta L_c = |cA'_c - cA_c|$
- High-frequency difference: $\Delta H_c = |H'_c - H_c|$

- 5) Compute the mean differences across all channels:

$$\Delta L = \frac{1}{3} \sum_{c \in \{R, G, B\}} \Delta L_c$$

$$\Delta H = \frac{1}{3} \sum_{c \in \{R, G, B\}} \Delta H_c$$

- 6) Calculate the ratio of perturbation in each frequency band:

$$\text{Low Frequency Ratio} = \frac{\text{Mean}(\Delta L)}{\text{Mean}(\Delta L) + \text{Mean}(\Delta H)} \times 100\%$$

$$\text{High Frequency Ratio} = \frac{\text{Mean}(\Delta H)}{\text{Mean}(\Delta L) + \text{Mean}(\Delta H)} \times 100\%$$

The visualizations were then created using Matplotlib with a unified color scale (copper colormap) to ensure fair comparison between different noise components.

Supplementary Materials: Visual-Friendly Concept Protection via Selective Adversarial Perturbations

APPENDIX

We show more cases of VCPro in Fig.13. VCPro can generate visually friendly perturbations while maintaining protection effectiveness.

Here we provide quantitative results to study the influence of hyper-parameters: training iteration, c , and α . We also provide qualitative results in supplementary materials. **Sensitivity Analysis of Training Iteration.** Usually, the larger the training steps, the larger the value of \mathcal{L}'_{θ} at different time steps, and the more successful the protection is. As shown in Fig. 14 (a), when increasing the number of training iterations, FID will first improve rapidly and then rise slowly, and the overall trend is that the longer the training iterations, the worse the quality of the protected image. Whereas LIQE will fall rapidly and then level off, the protection effect will improve and then remain stable. Finally, we selected 720 iterations based on the inflection point observed in Fig. 14 (a). At this point, we achieve substantial protection effectiveness (LIQE-SUM 4.37) while maintaining reasonable image quality (FID 27.04), and Fig. 15 also shows similar phenomena. Increasing iterations beyond 720 provides only marginal improvements in protection while continuing to degrade image quality.

Sensitivity Analysis of c . c represents stronger constraints on perturbation visibility. As shown in Fig. 14 (b), increasing parameter c reduces the FID score from 68.18 at $c = 0.0$ to 15.33 at $c = 1.0$, indicating significant improvements in visual quality of protected images. Meanwhile, protection effectiveness (LIQE-SUM) increases from 3.15 at $c = 0.0$ to 5.43 at $c = 0.5$, then slightly decreases to 4.75 at $c = 1.0$. Fig. 16 presents qualitative results across different c values, demonstrating that smaller c values (e.g., $c = 0.0$) provide stronger protection but compromise visual quality, while larger c values (e.g., $c = 1.0$) lead to friendly visibility with reduced protection. Based on analysis, we selected $c = 0.1$ as the optimal value, balancing acceptable protection effectiveness with maintainable visual quality.

Sensitivity Analysis of Parameter α . Fig. 17 (a) illustrates the impact of α on visual quality and protection effectiveness. Increasing α from 0 to 0.005 sharply increases FID from 0 to 33.93 (indicating more noticeable perturbations) while decreasing LIQE-SUM from 7.56 to 4.39 (indicating enhanced protection). Further increases to $\alpha = 0.020$ continue improving FID to 44.21 but result in saturated protection effectiveness (LIQE-SUM 3.55). Fig. 17 (b) shows that larger α values (e.g., 0.015, 0.020) require significantly more training iterations (1000) to converge compared to smaller values (e.g., $\alpha = 0.005$ requiring 80 iterations). Qualitative results in Fig. 18 show similar trends. We set $\alpha = 0.005$, which balances among visual quality, protection effectiveness, and computational efficiency.

Note that Fig. 17 uses $c = 0.005$ to clearly demonstrate the relationship between α and training iterations, as α values at $c = 0.1$ remain around 0.005 across the 240-1200 iteration range, making visualization challenging. In practice, to facilitate parallel acceleration, we adjust training steps to influence α . For each RGB image I , we performed the following analysis:

- 1) Apply 2D DWT to each color channel $c \in \{R, G, B\}$ separately:

$$\text{DWT}_c = \text{dwt2}(I_c, \text{'haar'})$$

- 2) Extract the approximation coefficients (low-frequency component) cA_c and detail coefficients (high-frequency components) cH_c , cV_c , and cD_c :

$$\text{DWT}_c = (cA_c, (cH_c, cV_c, cD_c))$$

- 3) Compute the combined high-frequency magnitude for each channel:

$$H_c = \sqrt{cH_c^2 + cV_c^2 + cD_c^2}$$

- 4) Calculate the frequency differences between clean image I and protected image I' :

- Low-frequency difference: $\Delta L_c = |cA'_c - cA_c|$
- High-frequency difference: $\Delta H_c = |H'_c - H_c|$

- 5) Compute the mean differences across all channels:

$$\Delta L = \frac{1}{3} \sum_{c \in \{R, G, B\}} \Delta L_c$$

$$\Delta H = \frac{1}{3} \sum_{c \in \{R, G, B\}} \Delta H_c$$

- 6) Calculate the ratio of perturbation in each frequency band:

$$\text{Low Frequency Ratio} = \frac{\text{Mean}(\Delta L)}{\text{Mean}(\Delta L) + \text{Mean}(\Delta H)} \times 100\%$$

$$\text{High Frequency Ratio} = \frac{\text{Mean}(\Delta H)}{\text{Mean}(\Delta L) + \text{Mean}(\Delta H)} \times 100\%$$

The visualizations were then created using Matplotlib with a unified color scale (copper colormap) to ensure fair comparison between different noise components.



Fig. 13. More qualitative defense results. For generating protected images, we use an ϵ value of $8/255$ with Stable Diffusion v1-4. Each row displays the original images (No Defense), the protected images generated our method, along with respective outcomes in Textual Inversion (TI) and DreamBooth (DB). For better detail, please zoom in.

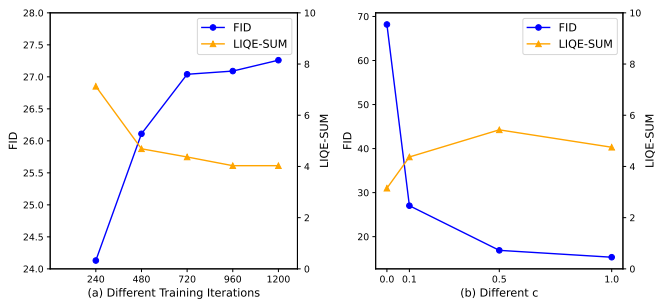


Fig. 14. Sensitivity analysis of hyper-parameters training iterations and c . FID is calculated between adversarial data and corresponding clean data; here LIQE-SUM is the sum LIQE of Textual Inversion and DreamBooth, which are all the smaller the better. The dataset is VGGface2 and $\epsilon = 8/255$.

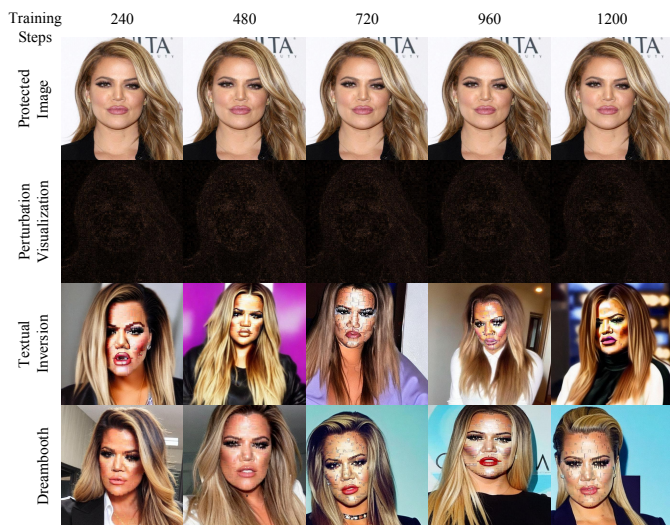


Fig. 15. Qualitative results for different training steps. For generating protected images, we use an ϵ value of $8/255$ with Stable Diffusion v1-4. For better detail, please zoom in.

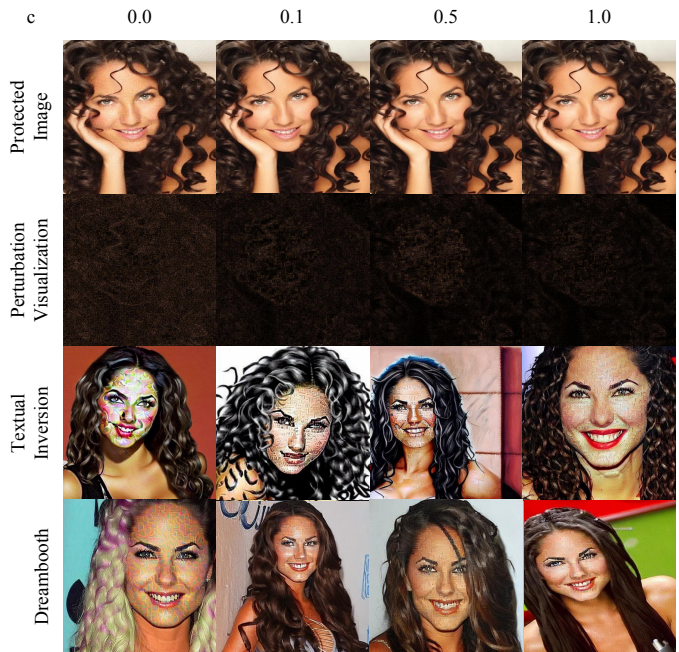


Fig. 16. Qualitative results for different c . For generating protected images, we use an ϵ value of $8/255$ with Stable Diffusion v1-4. For better detail, please zoom in.

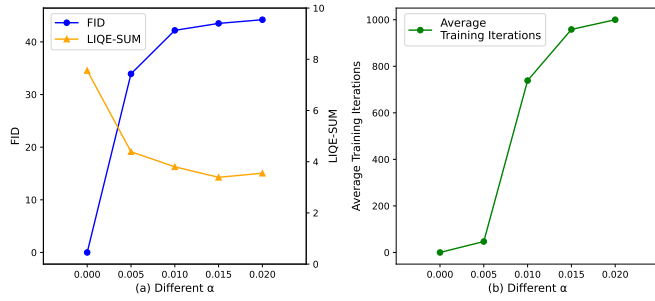


Fig. 17. Sensitivity analysis of hyper-parameter α . FID is calculated between adversarial data and corresponding clean data; here LIQE-SUM is the sum LIQE of Textual Inversion and DreamBooth, which are all the smaller the better. The dataset is VGGFace2 and $\epsilon = 8/255$.

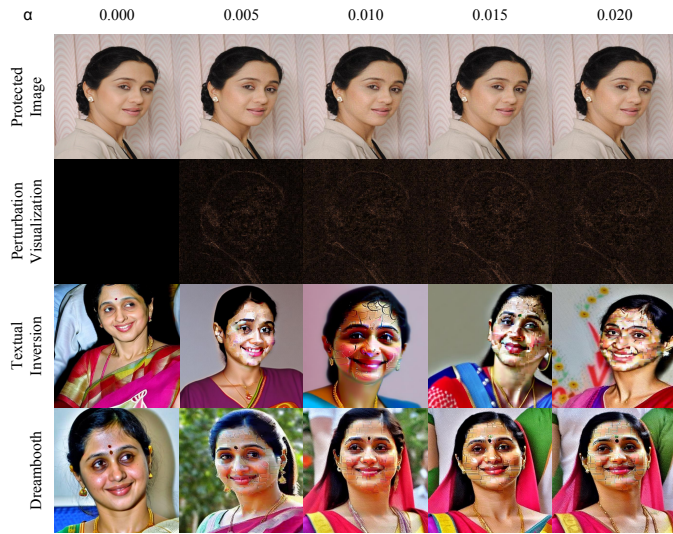


Fig. 18. Qualitative results for different α . For generating protected images, we use an ϵ value of $8/255$ with Stable Diffusion v1-4. For better detail, please zoom in.